The Astrophysical Journal, 664:322–331, 2007 July 20


# THE STAR-FORMING REGION NGC 346 IN THE SMALL MAGELLANIC CLOUD WITH *HUBBLE SPACE TELESCOPE* ACS OBSERVATIONS. II. PHOTOMETRIC STUDY OF THE INTERMEDIATE-AGE STAR CLUSTER BS 90[1]

Boyke Rochau and Dimitrios A. Gouliermis
Max Planck Institute for Astronomy, Königstuhl 17, 69117 Heidelberg, Germany;
rochau@mpia-hd.mpg.de, dgoulier@mpia-hd.mpg.de

Wolfgang Brandner
UCLA, Division of Astronomy, 475 Portola Plaza, Los Angeles, CA 90095-1547; and Max Planck Institute for Astronomy,
Königstuhl 17, 69117 Heidelberg, Germany; brandner@astro.ucla.edu, brandner@mpia-hd.mpg.de

Andrew E. Dolphin
Raytheon Corporation; adolphin@raytheon.com

and

Thomas Henning
Max Planck Institute for Astronomy, Königstuhl 17, 69117 Heidelberg, Germany; henning@mpia-hd.mpg.de
*Received 2007 March 20; accepted 2007 April 20*

## ABSTRACT

We present the results of our investigation of the intermediate-age star cluster BS 90, located in the vicinity of the H II region N66 in the SMC, observed with *HST* ACS. The high-resolution data provide a unique opportunity for a very detailed photometric study performed on one of the rare intermediate-age rich SMC clusters. The complete set of observations is centered on the association NGC 346 and contains almost 100,000 stars down to $V \simeq 28$ mag. In this study we focus on the northern part of the region, which covers almost the whole stellar content of BS 90. We construct its stellar surface density profile and derive structural parameters. Isochrone fits on the CMD of the cluster results in an age of about 4.5 Gyr. The luminosity function is constructed and the present-day mass function of BS 90 has been obtained using the mass-luminosity relation, derived from the isochrone models. We found a slope between $-1.30$ and $-0.95$, comparable to or somewhat shallower than a typical Salpeter IMF. Examination of the radial dependence of the mass function shows a steeper slope at larger radial distances, indicating mass segregation in the cluster. The derived half-mass relaxation time of 0.95 Gyr suggests that the cluster is mass segregated due to its dynamical evolution. From the isochrone model fits we derive a metallicity for BS 90 of $[\mathrm{Fe/H}] = -0.72$, which adds an important point to the age-metallicity relation of the SMC. We discuss our findings on this relation in comparison to other SMC clusters.

*Subject headings:* galaxies: clusters: individual ([BS95] 90) — Hertzsprung-Russell diagram — Magellanic Clouds — stars: evolution

## 1. INTRODUCTION

Studies of star clusters covering a wide range of ages, metallicities, and environments offer the opportunity to investigate the evolution of individual clusters, but also that of the entire parent galaxy, e.g., its star formation history and chemical enrichment. The clusters of the Large and Small Magellanic Clouds (LMC, SMC) are excellent targets for such studies. Their proximity allows us to resolve individual members of a stellar system and to assume that all stars of a star cluster are more or less located at the same distance. Studies of cluster systems of both the LMC and SMC provide the opportunity to test theories of stellar evolution for different ages, abundances, and/or mass contents in an environment different from the Milky Way. Star clusters of the Magellanic Clouds have ages varying from the early stages of the clouds up to the present, thereby allowing the study of the evolution of the clouds from the time they have been formed until today.

The history of cluster formation in the SMC is a topic of ongoing discussion. Although the cluster population has been considered as having a continuous age distribution (Da Costa & Hatzidimitriou 1998; Mighell et al. 1998), some studies suggest that most of the SMC clusters have been formed in two epochs. Rich et al. (2000) found seven populous SMC star clusters being formed either around $8 \pm 2$ Gyr or around $2 \pm 0.5$ Gyr ago. Rafelski & Zaritsky (2005) further argue that the cluster age distribution shows a few peaks, but no evidence for a significant age gap in the SMC as observed in the LMC (van den Bergh 1991; Da Costa 1991; Westerlund 1997). They suggest that the dominant initial epoch of cluster formation together with a fast dissolution of clusters gives an age distribution of the SMC clusters with a quiescent cluster formation period in the intermediate-age range. Consequently, the intermediate-age range in the SMC is sparsely populated.

The low number of intermediate-age SMC clusters makes it difficult to establish a consistent model for its chemical enrichment history. Pagel & Tautvaišiené (1998) published two models to explain the enrichment of the cluster populations of both the SMC and LMC. Their work includes a "bursting" model of star formation and a model with "smooth" star formation. For the latter, a constant star formation rate is assumed over the entire lifetime of the clouds. It is comparable to a model that has previously been published by Da Costa & Hatzidimitriou (1998).

[1] Research supported by the Deutsche Forschungsgemeinschaft (German Research Foundation).

The bursting model assumes a constant star formation rate over a certain time interval with a discontinuous change between two bursts. Pagel & Tautvaišienė (1998) included two bursts for the SMC, one at the time of its formation and the second at ~2.5 Gyr ago. Ages and metallicities of the cluster population have been examined with photometric analyses (e.g., Mighell et al. 1998; Piatti et al. 2001, 2005b) or via spectroscopy (e.g., Da Costa & Hatzidimitriou 1998; de Freitas Pacheco et al. 1998; Piatti et al. 2005a). The results of these studies are not providing a clear picture of the chemical enrichment of the SMC. As an example, results from Mighell et al. (1998) are in better agreement with the burst model of Pagel & Tautvaišienė (1998), whereas Da Costa & Hatzidimitriou (1998) pointed out that their findings are consistent with a more continuous chemical evolution following a simple "closed box" model for the SMC, but they also mentioned that it may be an "open" rather than a closed box due to its interaction with the LMC and the Galaxy. Naturally, the further investigation of intermediate-age star clusters would help to clarify the history of the cluster population of the SMC.

Recent high-resolution imaging with the Advanced Camera for Surveys (ACS) on board the *Hubble Space Telescope* (*HST*) of the general area of the stellar association NGC 346 in the SMC includes the intermediate-age star cluster BS[95] 90 (Bica & Schmitt 1995), or in short BS 90, providing, thus, a unique opportunity to study one of the very rare star clusters that was formed in a possible quiescent epoch of star formation in the SMC. Such high-resolution studies are quite rare. The catalog of SMC clusters imaged with the Wide-Field Planetary Camera 2 on board *HST* presented by Mackey & Gilmore (2003b) includes only 10 clusters, seven of which have ages between 12 and 1.4 Gyr. The study we present here on the cluster BS 90 is based on a unique set of deep observations toward an SMC cluster with the high resolving power of *HST* ACS. BS 90 is located in the vicinity of the stellar association NGC 346, the largest stellar concentration in the SMC, which is related to LHA 115–N66 (in short N66), the brightest H II region of the galaxy (Henize 1956). NGC 346 has been the subject of several studies. Peimbert et al. (2000) studied the chemical composition of the region. High-sensitivity CO and $H_2$ observations and imaging in [O III] of the photodissociation region is presented by Rubio et al. (2000). The X-ray emission in the general area has been studied by Nazé et al. (2003, 2004). Finally, a snapshot of the star formation history of the entire region is recently presented by Sabbi et al. (2007).

In the first paper of our investigation of the region of NGC 346 with *HST* ACS observations (Gouliermis et al. 2006, hereafter Paper I), we presented our photometry and the spatial distribution of different stellar populations in the whole region, revealing the stellar richness of the cluster BS 90. Our photometry allowed the resolution of stars down to $V \simeq 28$ mag (≈5 mag below the turnoff), corresponding to ~0.4 $M_\odot$. Naturally, the inclusion of BS 90 in this data set offers the opportunity for a detailed analysis of this unique cluster using one of the richest stellar samples in the SMC. Here we present our results of such an analysis. The structure of the paper is as follows. In § 2 we discuss the data set and the data reduction. The construction and analysis of the stellar surface density of the cluster is presented in § 3. In § 4 the color-magnitude diagram (CMD) of BS 90 is constructed and its properties are derived by isochrone fitting. In § 5 the luminosity and mass functions of the cluster are constructed and presented, and in § 6 we investigate the radial dependence of the mass function to examine a possible mass segregation. We discuss our findings concerning the age and metallicity of BS 90 in terms of the chemical enrichment history of the SMC in § 7. Finally, in § 8 we summarize our investigation of this unique SMC cluster.

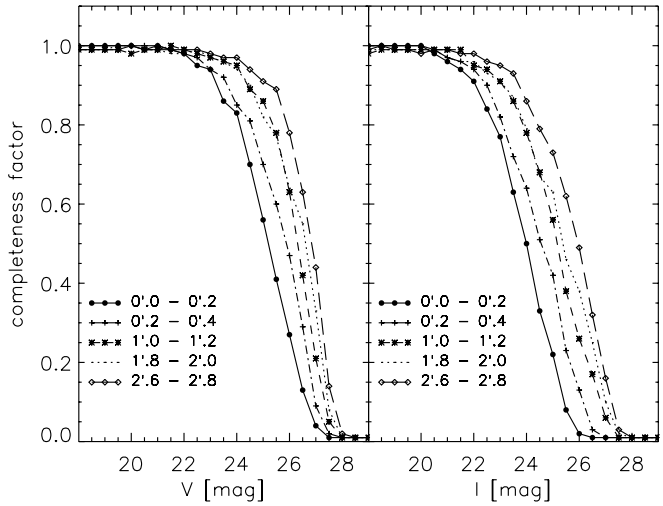


Fig. 1.—Completeness functions in $V$ (*left*) and $I$ (*right*) for five different distances from the center of the cluster. Annuli with radii of 0.0′–0.2′, 0.2′–0.4′, 1.0′–1.2′, 1.8′–2.0′, and 2.6′–2.8′ have been selected.

## 2. DATA DESCRIPTION AND ANALYSIS

The data we use in this study are collected within *HST* program GO-10248. Three pointings were observed using the Wide-Field Channel of ACS, centered on the association NGC 346, with the broadband filters F555W and F814W, equivalent to the standard $V$ and $I$, respectively. The data sets are retrieved from the *HST* Data Archive. Photometry of the pipeline-reduced FITS files was performed using the ACS module of the package DOLPHOT (ver. 1.0). This mode of the package is an adaption of HSTphot (Dolphin 2000), especially designed for photometry on ACS imaging. With our photometry we detected almost 100,000 stars. A detailed description of the data sets and a full account of the photometric process are given in Paper I, where we also made the whole photometric stellar catalog available.

This catalog lists the celestial coordinates and $V$ and $I$ magnitudes (in the Vega system) with the corresponding photometric errors for each star. Typical photometric uncertainties as a function of the magnitude are shown in Figure 2 of Paper I. The completeness of the data has been calculated by running DOLPHOT in artificial-star mode as described in Paper I, and artificial star lists were created with the utility `acsfakelist`. Completeness depends on the level of crowding, and consequently, in a populous compact cluster like BS 90 it should vary with respect to the distance from the center of the cluster, where crowding is higher. Indeed, the completeness in the area of BS 90 is found to be spatially variable. This is seen in Figure 1, where the completeness function in $V$ and $I$ (with the completeness factors estimated as a function of magnitude as $N_{\rm detected}/N_{\rm simulated}$) is shown for different selected distances from the center of the cluster.

## 3. DYNAMICAL BEHAVIOR OF THE CLUSTER

### 3.1. *Stellar Surface Density Profile of BS 90*

The observed field covers a quite large area around BS 90, allowing the construction of the stellar surface density profile of the cluster at relatively large distances from its center. We divided the area of the cluster into 30 concentric annuli with steps of 6″ and we counted the number of stars within each annulus. We corrected the counted stellar numbers for incompleteness according to the corresponding completeness factors. Completeness is a function of both distance from the center of the cluster and

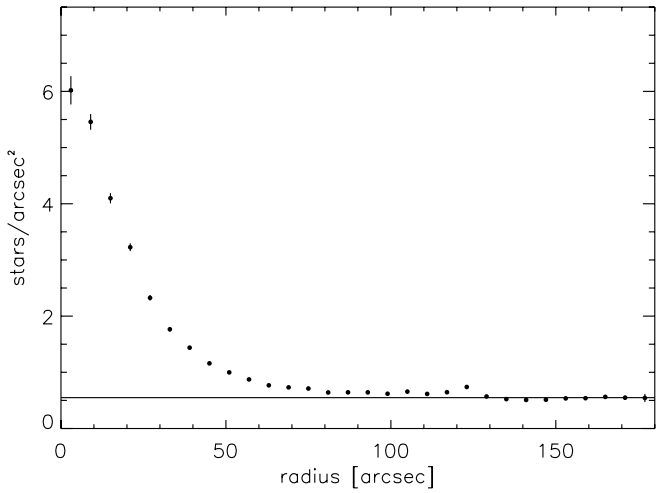


FIG. 2.—Radial stellar surface density profile. The stellar numbers have been corrected for incompleteness. The solid line shows the uniform level of the stellar background density, which corresponds to a value of ~0.55 stars arcsec$^{-2}$. The errors represent the uncertainties due to Poisson statistics. The small density peak at distance ~120″ is due to a young compact cluster to the east of BS 90.

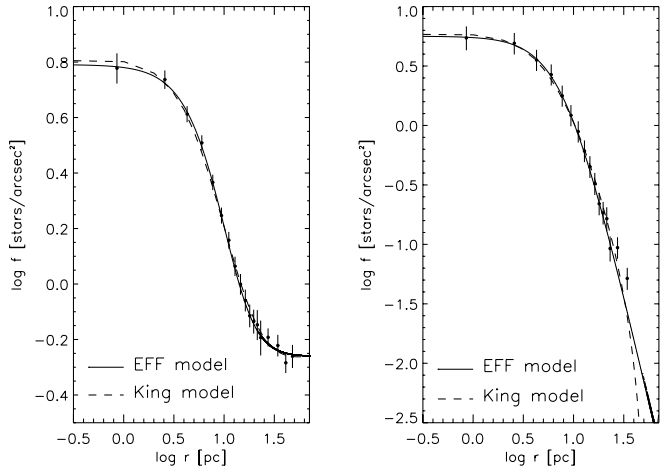


FIG. 3.—Radial surface density profile of BS 90 with the best-fitting King and EFF models superimposed. The King model is overplotted with a dashed line and the EFF model with a solid line. The error bars represent Poisson statistics. *Left*: Profile with all detected stars, including field and association. *Right*: Profile of the cluster alone after subtracting the estimated background density level. Both models fit very well the density profiles with a core radius of $r_c \simeq 5.6$ pc (EFF) or $r_c \simeq 5.4$ pc (King), a power-law slope of $\gamma = 3.68$ (EFF), and a tidal radius of $r_t \simeq 53.7$ pc (King).

magnitude. If $N_i(V)$ is the number of detected stars in the $V$ band within the $i$th annulus and in the brightness range corresponding to the completeness factor $c_i(V)$, the completeness-corrected number of stars is

$$N_{i,c} = \sum_V c_i(V) N_i(V). \quad (1)$$

We obtained the stellar surface density $f_i$ by normalizing this number to the area of the corresponding annulus as $f_i = N_{i,c}/A_i$, with $A_i$ being the area of the $i$th annulus. The observed field of view does not fully cover the northern and western extent of the cluster, and therefore for the annuli not completely observed, we considered only the available area for the estimation of the corresponding surface.

The constructed stellar surface density profile is shown in Figure 2. The errors correspond to uncertainties due to the counting process and they represent the Poisson statistics. As expected, this density profile shows a smooth drop as a function of distance from the center of the cluster. It drops to a uniform level, with the exception of the small increase at the distance around 2′. We identify this increase as a small young cluster located east of BS 90. The horizontal uniform level represents the stellar density of the field of the galaxy. Its value is shown as the solid line in Figure 2 and has been measured by fitting the models of Elson et al. (1987) to the stellar surface density profile, as shown below.

### 3.2. *Structural Parameters*

We applied both the empirical model by King (1962) and the model of Elson et al. (1987; hereafter "the EFF model") to the stellar surface density profile of BS 90 in order to obtain its structural parameters. The EFF model is suited for clusters without tidal truncation, while King's empirical model represents a tidally truncated cluster. Both models provide the opportunity to derive accurate characteristic radii for the cluster, such as its core and tidal radius. The core radius ($r_c$) describes the distance from the center of the cluster where the stellar density drops to the half of its central value, and the tidal radius ($r_t$) is the limit where the density drops to zero. For the application of King's model the stellar surface density of the cluster alone (with no contamination from the field) is necessary, while the EFF model does not require any field subtraction. We first apply the latter in order to estimate the core radius and the uniform background level. The subtraction of this density level from the measured surface density at each annulus gives the surface density profile of the cluster alone, from which we derive the core and tidal radii.

#### 3.2.1. *Best-Fitting EFF Profile*

From studies of young LMC clusters by EFF it appears that the examined clusters are not tidally truncated. These authors developed a model more suitable to describe the stellar surface density profile of such clusters:

$$f(r) = f_0\left(1 + r^2/a^2\right)^{-\gamma/2} + f_{\rm field}, \quad (2)$$

where $f_0$ is the central stellar surface density, $a$ is a measure of the core radius, and $\gamma$ is the power-law slope that describes the decrease of surface density of the cluster at large radii [$f(r) \propto r^{-\gamma}$ for $r \gg a$]; $f_{\rm field}$ represents the uniform background density level. Our best fit of the EFF model to the surface density profile of BS 90 gives $a = 8.24 \pm 0.67$ pc and $\gamma = 3.68 \pm 1.05$. The density of the background field, taken from the fitting procedure, corresponds to a value of $f_{\rm field} \sim 0.55 \pm 0.04$ stars arcsec$^{-2}$. According to EFF model, the core radius $r_c$ is given by equation (2), assuming no contribution from the field, as

$$r_c = a\left(2^{2/\gamma} - 1\right)^{1/2}. \quad (3)$$

We estimate a core radius of $r_c = 5.57^{+0.73}_{-0.37}$ pc. The best-fitting EFF model assuming the derived values of $a$, $\gamma$, and $f_{\rm field}$ is shown superimposed on the stellar surface density profile in Figure 3.

#### 3.2.2. *Best-Fitting King Profile*

In order to have the density profile of the cluster alone we subtracted the background density level of ~0.55 ± 0.04 stars arcsec$^{-2}$, estimated above, from the profile of Figure 2. Then we used the field-subtracted profile to derive the core and tidal radius of the

cluster as described by King (1962). Specifically, according to this model the core radius is found from the formula

$$f = \frac{f_0}{1 + (r/r_c)^2}, \quad (4)$$

which describes the inner region of the cluster and the tidal radius from

$$f = f_1(1/r - 1/r_t)^2, \quad (5)$$

which represents the outskirts of the cluster. Here $f_0$ describes again the central surface density of the cluster and $f_1$ is a constant. The best-fitting profile results in a tidal radius $r_t = 53.66^{+8.93}_{-7.10}$ pc ($3.13^{+0.53}_{-0.41}$ arcmin) and a core radius $r_c = 5.44^{+0.33}_{-0.35}$ pc ($19.06^{+1.15}_{-1.23}$ arcsec). The concentration parameter $c$ is defined as the logarithmic ratio of tidal to core radius $c = \log(r_t/r_c)$ and refers to the compactness of the cluster. We obtained a concentration parameter $c = 1.0 \pm 0.1$. According to King's model the density profile of a tidally truncated cluster is given as

$$f \propto \left\{ \frac{1}{[1 + (r/r_c)^2]^{1/2}} - \frac{1}{[1 + (r_t/r_c)^2]^{1/2}} \right\}^2, \quad (6)$$

where $f$ is the stellar surface density, $r_c$ and $r_t$ the core and tidal radii, respectively, and $r$ the distance from the center. The best-fitting King model is shown as the dashed line, superimposed on the radial surface density profile in Figure 3.

Both King and EFF models are in good agreement with each other. The intermediate region is equally well fitted by both models. Based on the accuracy of the fits, it can be concluded that the EFF model is in better agreement with our data in the inner part of the cluster, but for the intermediate and outer regions of the cluster the best fits yield no preference for the tidally truncated King model or the EFF model.

### 3.2.3. *Core Radius–Age Relation of SMC Clusters*

A comparison of 10 SMC clusters, investigated by Mackey & Gilmore (2003b), shows that they can be divided into two groups with respect to their core radii, as they are derived from the EFF model. One group contains six star clusters (NGC 176, 330, 121, 411, 416, and 458) with radii less than 5 pc, and the second group includes the remaining four clusters (NGC 361, 152, and 339 and Kron 3) with $r_c > 5$ pc. BS 90 with its core radius of $r_c = 5.57$ pc, as found from EFF models, would be a member of the second group. Mackey & Gilmore examined the relationship between the core radii and the ages of clusters located in the LMC, SMC, Fornax, and Sagittarius dwarf spheroidals (see Mackey & Gilmore 2003a, 2003b, 2003c), and in Figure 4 the core radius–age relationship for the SMC cluster sample is shown with our measurements for BS 90. The distinction of the clusters into the two groups according to their core radii is easily seen in this plot. For the LMC and the Fornax and Sagittarius dwarf spheroidals they observed a similar distinction and argued that it shows a real evolution of cluster structure with age (Mackey & Gilmore 2003a, 2003c), with the sequence of clusters with smaller core radii following the "standard" isolated globular cluster evolution. These authors suggest that the evolution of the clusters in the upper right of Figure 4, where BS 90 belongs, differs from this isolated evolution. The disparity could be due to very different stellar populations in these clusters or because they do not follow an isolated evolution, but rather an evolution influenced by external processes.

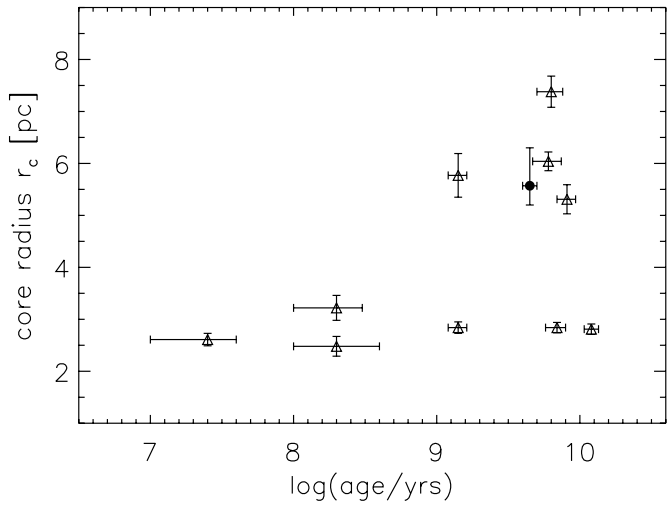


Fig. 4.—Core radius vs. age for the SMC clusters examined by Mackey & Gilmore (2003b), with the values for BS 90 found in this paper also plotted. The triangles represent the clusters that have been investigated by Mackey & Gilmore (2003b). The star cluster BS 90 is displayed as the black dot. Clusters that are located in the upper right may have not been evolved in isolation.

McLaughlin & van der Marel (2005) also derived core and tidal radii with the application of King empirical models, and the same separation of the clusters into the two groups according to their core radii was observed in their sample. Our application of King empirical models yields a core radius of $r_c \simeq 5.4$ pc and a tidal radius of $r_t \simeq 53.7$ pc, making BS 90 also a member of the second group of the McLaughlin & van der Marel sample of clusters. Our estimated concentration parameter for BS 90 $c \simeq 1.0$ is relatively low in comparison to the SMC clusters studied by Mackey & Gilmore (2003b) and McLaughlin & van der Marel (2005).

### 3.2.4. *Half-Light Radius*

The half-light radius of the cluster is derived from its surface brightness profile. It corresponds more or less to the half-mass radius, and the corresponding half-mass relaxation time (§ 6.1) is a useful reference time for the dynamical evolution of the cluster as a whole (Spitzer 1987). To construct the surface brightness profile we subdivided the area of the cluster into 26 annuli. The first 22 annuli were selected in steps of 6″ and the remaining four in steps of 12″. We changed the width of the annuli to improve the statistics in the outer regions of the cluster. We converted the measured apparent magnitudes into flux and counted the brightness of the stars within each annulus. The total brightness of each annulus has been corrected for incompleteness and normalized to the corresponding area. From our fit of the profile with the EFF model we derived the total brightness of the entire cluster and further obtained its half-light radius. We found a half-light radius of $r_h = 9.42 \pm 0.5$ pc.

## 4. COLOR-MAGNITUDE DIAGRAM

The $V - I$ versus $V$ color-magnitude diagram (CMD) of all stars detected within a circular area of two core radii around the center of the cluster is shown in Figure 5. A comparison of the contour maps of the region around NGC 346, constructed with star counts in Paper I, shows that the main body of the cluster covers well the northern part of the observed field of view (Paper I, Fig. 4). Our selected radius of $2r_c$ around the center of BS 90 corresponds to 11.15 pc and is comparable to the half-light radius of 9.42 pc. It contains more than 40% of the total number of

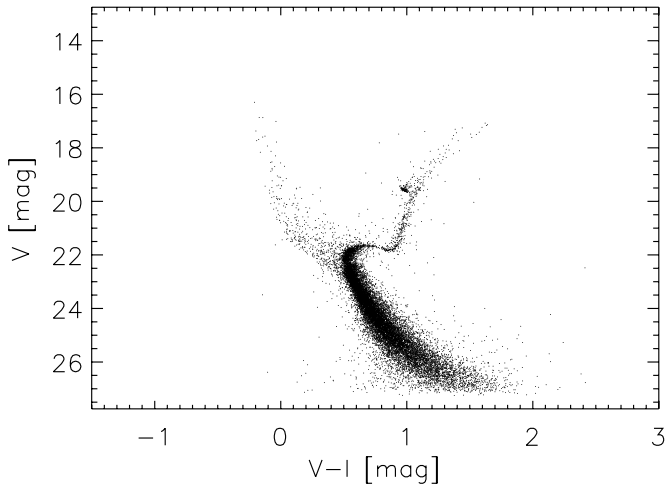


FIG. 5.—$V$, $V-I$ CMD of all detected stars within a circular area of $2r_c$, corresponding to ~11.2 pc, around the center of the cluster BS 90. The turnoff is clearly visible and the features of the RC, the SGB, and the RGB are easily seen as well, making BS 90 a bona fide case. This CMD is contaminated by field stars and also by the close-by association NGC 346, the population of which is apparent in the upper main sequence with colors bluer than $V-I \lesssim 0.5$ mag.

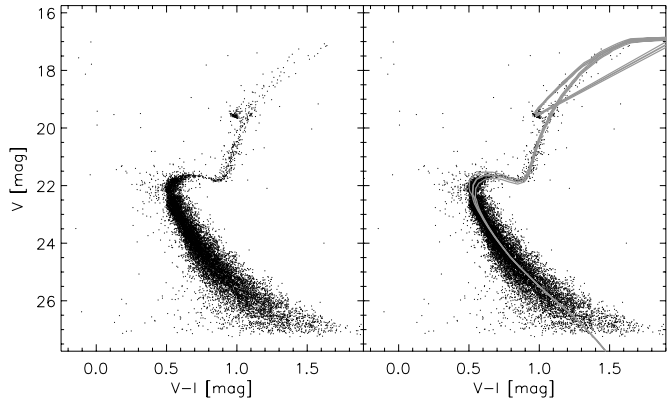


FIG. 6.—*Left*: $V$, $V-I$ CMD of BS 90 after the contaminating stellar population of the general SMC field and the association NGC 346 has been randomly subtracted with the Monte Carlo method. The contaminating stars of the upper main sequence are almost completely removed. Remaining stars with 21.5 mag $\lesssim V \lesssim$ 22.5 mag and 0.2 mag $\lesssim V-I \lesssim$ 0.6 mag may indicate a population of blue stragglers. *Right*: The same CMD with the applied isochrone models overplotted. The best-fitting isochrone, plotted by the middle thick line, gives an age of $\tau \simeq 4.5$ Gyr. The remaining two models, plotted with thin lines, correspond to the limiting isochrones that can also be fitted, and provide the error of 0.5 Gyr in the age estimation. All three models fit the cluster best for a metallicity [Fe/H] $\simeq -0.72$, an assumed distance modulus of $m-M \simeq 18.85$ mag, and a total visual extinction $A_V \sim 0.04$ mag. The features of the RC, the RGB, the SGB, and the turnoff are all fitted accurately.

observed stars and more than 60% of the observed cluster population. The CMD of Figure 5 is indicative of an old cluster with a clear turnoff at $V \sim 22$ mag and $V-I \sim 0.5$ mag, a well-defined subgiant branch between 0.6 mag $\lesssim V-I \lesssim$ 1.0 mag and $V \sim 21.5$ mag, a red giant branch between 1.0 mag $\lesssim V-I \lesssim$ 1.65 mag and 17 mag $\lesssim V \lesssim$ 21.5 mag, and a populated red clump at $V \sim 19.5$ mag and $V-I \sim 1.0$ mag. The CMD naturally includes also field stars and stars of the nearby young association NGC 346 (see also Paper I). Part of the latter is visible, for instance, as the population of the upper main sequence.

### 4.1. *Subtraction of Contaminating Stars*

In order to have a "clean" CMD, composed only of stars of the cluster, the subtraction of all contaminating populations is necessary. Therefore we applied a Monte Carlo subtraction method to clean the diagram of stars that belong to the field and the association.

Naturally, this subtraction might depend on the area chosen to be field. Considering that the observed field of view is no more than $5' \times 5'$ in size, and that the association NGC 346 itself also contaminates the stellar population of BS 90, we tested several "empty" areas within the field of view, which also include stars from the association, as potential fields, in order to determine the most realistic stellar numbers that should be reduced from the CMD of BS 90. As a reference for the stellar contamination we selected an area of $75'' \times 50''$ in the south of BS 90 with its center ~90″ away from the center of the cluster. It contains stars of the association and of the general field, and also a few stars of the cluster itself. The number of stars that belong to the cluster is negligible at distances of $r > 65''$ from its center, because the stellar surface density has almost dropped to the background level of the field at this distance (see Fig. 2). We made the assumption that the selected area contains only field stars and stars of the association and not stars of BS 90. This leads to a small overestimation of the number of stars to be subtracted and causes a slightly higher number of subtractions in the area of the subgiant branch and the main sequence.

We divided the CMD into a grid and counted the numbers of stars in each grid element of the CMD of the reference field. Considering that the field subtraction might also depend on the size of the elements, we tested the Monte Carlo subtraction for different grid element sizes, and we found that a size of 0.125 mag is the most suitable. Smaller element sizes produce poor number statistics, while larger sizes result in rough field-subtracted CMDs. Furthermore, we considered the different completeness of the two regions by correcting the corresponding stellar numbers for every field. Finally, we normalized the stellar numbers to the selected area of the cluster. The resulting number of stars that contaminate the CMD of BS 90 has been removed. The stars that have been excluded have been randomly selected from the corresponding bin of the original CMD of Figure 5. The derived "clean" CMD of BS 90 with no contamination by other stellar populations is shown in Figure 6.

### 4.2. *The CMD of the Cluster*

The CMD of Figure 6 (*left*), which corresponds to the CMD of the star cluster BS 90 alone, shows features of a bona fide intermediate-age cluster. The diagram reveals a well-populated faint main sequence, as well as a clear turnoff. Well-defined features are also the subgiant branch (SGB), the red giant branch (RGB), and the red clump (RC). The asymptotic giant branch is sparsely populated. These clear characteristics of the cluster allow isochrones to be easily used in order to define several properties of BS 90. Specifically, the SGB, the RGB, and the RC show no significant differential reddening, which makes the application straightforward. We used isochrone models calculated by the Padova group (Girardi et al. 2002) in the VEGA filter system for the ACS filters.

The best-fitting isochrones are shown in the right panel of Figure 6 superimposed on the CMD. The chosen isochrone fits very well the turnoff, RC, SGB, and RGB. These well-defined features of BS 90 allow us to make an accurate estimation of the characteristic properties of the cluster:

1. *Age and metallicity.*—The best-fitting isochrones from the model grid used give an age of $4.5 \pm 0.5$ Gyr and a metallicity of $Z = 0.004 \pm 0.001$. This metallicity leads through the relation $[\mathrm{Fe/H}] = 1.024 \log Z + 1.739$ (Bertelli et al. 1994) to an iron content for BS 90 of $[\mathrm{Fe/H}] = -0.72^{+0.10}_{-0.13}$.

2. *Reddening and distance*.—From our isochrone fit we found a color excess of only $E(V-I) \simeq 0.016$ mag. Using the relation between the extinction in $V$, $A_V$, and the color excess $E(V-I)$, derived by Mackey & Gilmore (2003c), we obtained a total visual extinction of $A_V \simeq 0.038$ mag. We assumed a normal extinction law with a total-to-selective absorption of $R_V = 3.1$ (Binney & Merrifield 1998), which gives $E(B-V) \simeq 0.021$ mag.

The distance modulus of BS 90 has been determined to $m - M \simeq 18.85 \pm 0.1$ mag, which corresponds to a distance of $58.9 \pm 0.45$ kpc.

#### 4.2.1. *Blue Straggler Candidates*

As shown in the CMD of Figure 6, after the field subtraction there are still a few stars that remain located a bit above the turnoff and to the blue. These stars appear to be main-sequence stars with masses larger than expected for stars of the cluster at its turnoff age. The region of the CMD covered by these stars is between $V \simeq 22.5$ and 21 mag, comparable to the region on the CMD where blue straggler stars are found in the LMC cluster ESO 121–SC 03 (Mackey et al. 2006). The spatial distribution of these candidate blue stragglers in BS 90 shows that they are concentrated in the center of the cluster. This supports the suggestion that these stars represent indeed a blue straggler population, since such stars are centrally concentrated. A suggested explanation for the blue stragglers phenomenon is mass exchange in binary systems and merging processes, which increase the mass of one star and therefore it shines brighter and is bluer than expected for its age.

## 5. LUMINOSITY FUNCTION AND MASS FUNCTION

### 5.1. *Luminosity Function*

We constructed the $V$- and $I$-band luminosity functions (LFs) of the cluster, which are presented in Figure 7. For the construction of the LF we considered the CMD of the cluster shown in Figure 6, without the contamination by the populations of the association and the background field within a radius 2.8′ from the center of the cluster (comparable to $r_t$). We counted the stars in magnitude bins of 0.25 mag and corrected the numbers for incompleteness. The LF has been normalized to the considered surface of 6.5 arcmin$^2$. The completeness-corrected LF is shown with thick solid lines. The vertical dotted lines in Figure 7, which correspond to $V = 25.75$ mag and $I = 24.5$ mag, represent the 50% completeness limit. The vertical dash-dotted line at $V = 25$ mag and $I = 23.75$ mag corresponds to the 70% completeness limit. The dashed line shows the LF before the completeness correction.

In the LFs of Figure 7 different features of the cluster can be clearly identified. The RC is visible as the increase in stellar density around $V = 19.5$ mag. The turnoff is also distinguishable at $V \simeq 21.5$ mag. For fainter stars the LF turns into a linearly increasing function, showing the main-sequence stars of the cluster. In the case of the $I$-band LF we observe similar features. Around $I = 18.5$ mag we identify the RC, and we see the turnoff at $I \simeq 20.75$ mag. For stars with 20.75 mag $\lesssim I \lesssim 22$ mag the linear increase of the LF is steeper than for 22 mag $\lesssim I \lesssim$ 24.5 mag. The latter range is composed of stars on the main sequence.

### 5.2. *Mass Function*

The initial mass function (IMF) describes the mass distribution of a newly formed stellar population. The stellar mass function is changed under the influence of the stellar as well as dynamical evolution that affects entire stellar systems such as

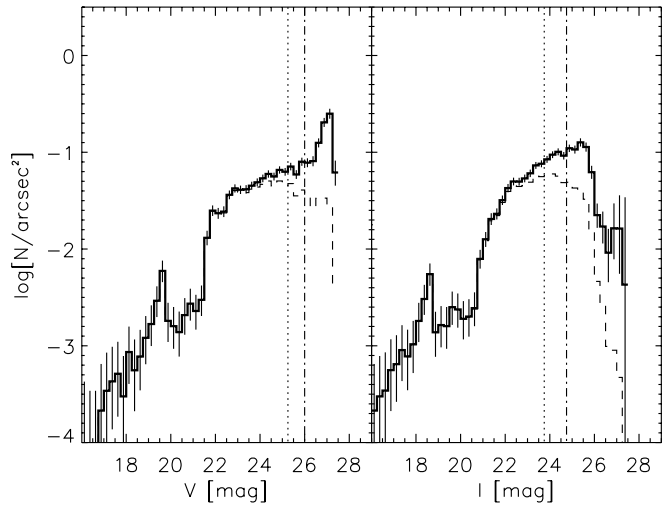


FIG. 7.—Field-subtracted LFs in $V$ (*left*) and $I$ (*right*) of the cluster within a radius 2.8′. The features of the RC around $V \sim 19$ mag and $I \sim 18.5$ mag and the turnoff at $V \sim 21.5$ mag and $I \sim 21$ mag are clearly seen. The increase of the stellar density for $V \gtrsim 26.5$ mag is probably due to the very low completeness in our data. The vertical dotted line represents the 70% completeness limit, while the vertical dash-dotted line represents the 50% completeness limit. The errors represent Poisson statistics. The dashed line shows the LF before it has been corrected for incompleteness.

star clusters (Baumgardt & Makino 2003). The present-day mass function (PDMF) is the result of such evolutionary effects. In general, the IMF can be described as a power law (Scalo 1986),

$$\xi(\log m) \propto m^{\Gamma}, \tag{7}$$

and represents the distribution of stellar masses for a given stellar system at the time of their formation. The index $\Gamma$ is its power-law slope:

$$\Gamma = \frac{d \log \xi(\log m)}{d \log m}. \tag{8}$$

Salpeter (1955) found a value for the slope of the IMF in the solar neighborhood, often taken as a reference, of $\Gamma = -1.35$. In the same manner as for the IMF, we describe the slope of the PDMF as

$$a = \frac{d \log N(\log m)}{d \log m}, \tag{9}$$

where $N(\log m)$ is the PDMF. This slope is given by the linear relation between the logarithmic mass intervals and the corresponding number of stars (in logarithmic scale). In order to obtain the PDMF of a cluster, knowledge of the mass-luminosity relation is required. In the case of BS 90, and since a single age model fits the cluster almost perfectly, we used the mass-luminosity relation taken from the 4.5 Gyr isochrone of Girardi et al. (2002) and ascribed the present mass to each star that belongs to our stellar sample of the cluster. To construct the PDMF of BS 90, we counted stars in logarithmic mass intervals and normalized their numbers to the considered area. We corrected these numbers for incompleteness.

The constructed PDMF is shown in Figure 8, where an almost linear increase to lower masses can be seen. The low- and high-mass ends of the PDMF show a steep increase and decrease, respectively. In the case of the low-mass end this is probably due to the completeness corrections, while for the high-mass end

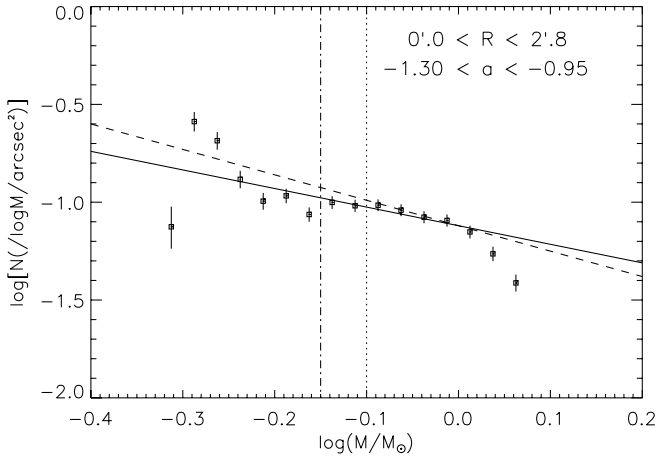


FIG. 8.—Field-subtracted, completeness-corrected PDMF of the cluster within a radial distance of 2.8′ from its center. The steep increase to the lower mass end [$\log(M/M_\odot) < -0.25$] is probably due to the very low completeness. The vertical dotted line represents the 70% completeness limit while the vertical dash-dotted line represents the 50% completeness limit. The best linear fit for data with completeness higher than 50%, corresponding to a slope of $a \simeq -0.95$, is plotted with a solid line. The dashed line shows the linear fit to the MF for stars with completeness higher than 70% with a slope of $a \simeq -1.30$.

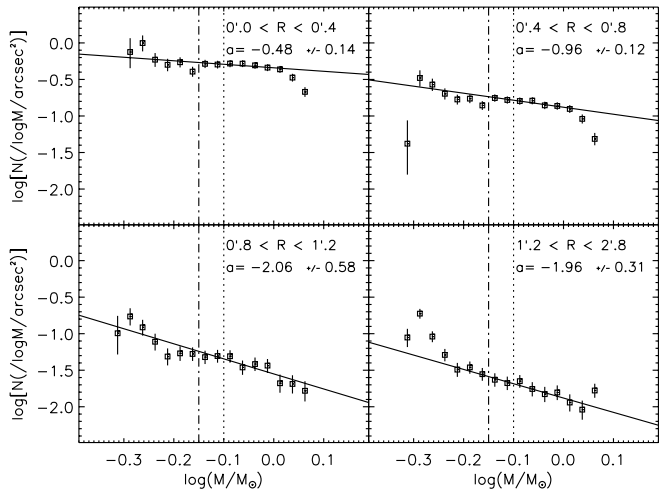


FIG. 9.—MFs of BS 90 for four selected radial distances (0.0′–0.4′, 0.4′–0.8′, 0.8′–1.2′, and 1.2′–2.8′). The dotted and dash-dotted lines represent the 70% and 50% completeness limits, respectively. The linear fits to the mass functions are represented by the solid line in each panel. The MF becomes steeper for larger radial distances from the center of the cluster, indicating that mass segregation takes place.

stellar evolution is possibly responsible. The 50% completeness limit corresponds to a mass of $M \sim 0.7\ M_\odot$ and is represented by the vertical dash-dotted line. The 70% completeness limit is shown with a vertical dotted line and represents a lower mass limit of $M \sim 0.8\ M_\odot$. The straight solid line shows the fit to the mass function (MF) above the 50% completeness limit, without the two highest mass points. The fit gives a single power-law slope of $a = -0.95 \pm 0.14$, a bit flatter than Salpeter's IMF, whereas the fit to the MF above the 70% completeness limit reveals a Salpeter-like slope of $a = -1.30 \pm 0.14$. It is represented by the dashed line.

Kroupa (2002) notes that theoretical examinations of the dynamics of massive and long-lived globular clusters ($N \gtrsim 10^5$ stars) reveal that the global PDMF is similar to the PDMF at distances near the half-mass radius. The PDMF inward and outward of the half-mass radius becomes flatter and steeper, respectively, due to dynamical mass segregation. Dynamical evolution of a cluster also flattens the global PDMF, since evaporation is stronger for stars with lower masses than for high-mass stars (Vesperini & Heggie 1997).

## 6. MASS SEGREGATION IN BS 90

The phenomenon of mass segregation describes the concentration of high-mass stars toward the center of a star cluster. This phenomenon could be either of primordial origin or the result of the dynamical evolution of the cluster. The latter effect leads the cluster to a state of energy equipartition between its stars. Therefore, stars with lower masses will have higher velocities and thus larger orbits. On the other hand, stars with higher masses have smaller orbits and concentrate toward the center. Indeed, stellar MFs at the outer parts of star clusters indicate the existence of more low-mass stars at larger radii than in the central region of the cluster (de Grijs et al. 2002). A powerful diagnostic for the detection of the phenomenon of mass segregation in a star cluster is its MF, which is expected to be radially variable if segregation is present (e.g., Gouliermis et al. 2004). Therefore, in order to see if BS 90 is mass segregated or not, we derived its MF for annuli at different radial distances from the center of the cluster. We derived the different MFs as described in § 5.2 for four selected radial distances: 0.0′–0.4′, 0.4′–0.8′, 0.8′–1.2′, and 1.2′–1.6′. The resulting MFs are shown in Figure 9. The MF of the innermost region has a slope of $a = -0.48 \pm 0.14$. The MF of the second annulus, which includes the half-light radius, is comparable to the MF inside 2.8′ shown in Figure 8 and has a slope of $a = -0.96 \pm 0.12$. The slopes of the outer regions are found to be steeper with $a = -2.06 \pm 0.58$ for 0.8′–1.2′ and $a = -1.96 \pm 0.31$ for 1.2′–2.8′. The difference of the MF slope being steeper outward gives clear evidence of mass segregation in BS 90. In the following section, we explore the driving mechanism of this phenomenon.

### 6.1. *Half-Mass Radius and Dynamical Timescale*

As mentioned above, the phenomenon of mass segregation may be primordial, due to the formation of the most massive stars in the central regions of the cluster, or an evolutionary effect due to the dynamical relaxation of the cluster. The latter is achieved via two-body encounters, which lead to a quasi-Maxwellian equilibrium in the interior of the cluster (Lightman & Shapiro 1978). The tendency of the inner regions of the cluster to reach thermal equilibrium leads to energy equipartition among different stellar mass groups and consequently to mass stratification. The timescale in which such equipartition is accomplished is given roughly by the relaxation time $t_{\rm rl}$ of the cluster (e.g., Spitzer 1975). Hence, the relaxation time can indicate whether a case of mass segregation is of dynamical origin (when the evolution time of the stellar system is longer than the relaxation time) or not. This timescale can be expressed as (Binney & Tremaine 1987)

$$t_{\rm rl} = \frac{6.63 \times 10^8}{\ln 0.4N} \left(\frac{M}{10^5\ M_\odot}\right)^{1/2} \left(\frac{M_\odot}{m_\star}\right) \left(\frac{R}{\rm pc}\right)^{3/2} {\rm yr}, \quad (10)$$

where $M$ is the total mass in a certain characteristic radius $R$, $m_\star$ is a characteristic mass (median mass of the observed stellar distribution), and $N$ is the corresponding number of stars of the system. The half-mass radius corresponds more or less to the half-light radius of the cluster. The half-light radius of BS 90 derived from its surface brightness profile (§ 3.2.4) is found to be equal to $r_h = 9.42 \pm 0.5$ pc. Following equation (10), we derive the

TABLE 1

Collective Data on Ages and Metallicities of Star Clusters in the SMC

| Name | R.A. | Decl. | Age (Gyr) | Metallicity [Fe/H] | References |
|---|---|---|---|---|---|
| NGC 121 | 00:26:49 | −71 32 10 | 12.00 ± 2.00 | −1.19 ± 0.12 | 1 |
| | | | 11.90 ± 1.30 | −1.71 ± 0.10 | 2 |
| | | | 12.00 ± 5.00 | −1.20 ± 0.32 | 3 |
| NGC 152 | 00 32 56 | −73 06 57 | 1.40 ± 0.20 | −0.94 ± 0.15 | 4 |
| | | | 1.90 ± 0.50 | −0.80 ± 0.30 | 1 |
| NGC 176 | 00 35 59 | −73 09 57 | $0.20^{+0.20}_{-0.10}$ | −0.60 | 5 |
| NGC 339 | 00 57 48 | −74 28 00 | 4.00 ± 1.50 | −1.19 ± 0.10 | 1 |
| | | | 6.30 ± 1.30 | −1.50 ± 0.14 | 2 |
| | | | 2.00 ± 0.70 | −0.70 ± 0.22 | 3 |
| NGC 361 | 01 02 13 | −71 36 16 | 8.10 ± 1.20 | −1.45 ± 0.11 | 2 |
| NGC 411 | 01 07 56 | −71 46 05 | 1.40 ± 0.20 | −0.68 ± 0.07 | 6 |
| | | | $1.30^{+0.50}_{-0.30}$ | −0.70 ± 0.22 | 3 |
| | | | 1.50 ± 0.30 | −0.70 ± 0.20 | 7 |
| | | | 1.80 ± 0.30 | −0.84 ± 0.30 | 1 |
| NGC 416 | 01 07 59 | −72 21 20 | 6.90 ± 1.10 | −1.44 ± 0.12 | 2 |
| | | | 4.00 ± 1.50 | −0.80 ± 0.23 | 3 |
| NGC 419 | 01 08 19 | −72 53 03 | 4.00 ± 1.50 | −0.60 ± 0.21 | 3 |
| | | | 1.20 ± 0.50 | −0.70 ± 0.30 | 1 |
| NGC 458 | 01 14 53 | −71 32 59 | 0.20 ± 0.10 | $-0.23^{+0.10}_{-0.40}$ | 1 |
| | | | 0.13 ± 0.06 | $-0.23^{+0.10}_{-0.40}$ | 7 |
| L1 | 00 04 00 | −73 28 00 | 10.00 ± 2.00 | −1.01 ± 0.11 | 1 |
| | | | 9.00 ± 1.00 | −1.35 ± 0.08 | 2 |
| L4 | 00 21 27 | −73 44 55 | 3.10 ± 0.90 | −0.90 ± 0.20 | 8 |
| L5 | 00 22 40 | −75 04 29 | 4.10 ± 0.90 | −1.20 ± 0.20 | 8 |
| | | | 3.00 ± 1.50 | −1.10 ± 0.20 | 7 |
| L6/K4 | 00 23 04 | −73 40 11 | 3.30 ± 0.90 | −0.90 ± 0.20 | 8 |
| L7/K5 | 00 24 43 | −73 45 18 | 2.00 ± 0.20 | −0.60 ± 0.20 | 8 |
| | | | 1.20 ± 0.50 | −0.50 ± 0.20 | 7 |
| L11/K7 | 00 27 45 | −72 46 53 | 3.50 ± 1.00 | −0.81 ± 0.13 | 1 |
| | | | 3.50 ± 0.50 | −1.00 | 7 |
| L19 | 00 37 42 | −73 54 30 | 2.10 ± 0.20 | −0.75 ± 0.20 | 8 |
| L27 | 00 41 24 | −72 53 27 | 2.10 ± 0.20 | −1.30 ± 0.30 | 8 |
| L32 | 00 47 24 | −68 55 10 | 4.80 ± 0.50 | −1.20 ± 0.20 | 9 |
| L38 | 00 48 50 | −69 52 11 | 6.00 ± 0.60 | −1.65 ± 0.20 | 9 |
| L113 | 01 49 30 | −73 43 40 | 6.00 ± 1.00 | −1.17 ± 0.12 | 1 |
| | | | 5.30 ± 1.30 | −1.24 ± 0.11 | 2 |
| L116 | 01 55 33 | −77 39 16 | 2.80 ± 1.00 | −1.10 ± 0.20 | 9 |
| K3 | ... | ... | 6.00 ± 1.30 | −1.16 ± 0.09 | 2 |
| | | | 9.00 ± 2.00 | −0.98 ± 0.12 | 1 |
| | | | 3.50 ± 1.50 | −1.00 ± 0.28 | 3 |
| | | | 7.00 ± 1.00 | −1.20 ± 0.20 | 7 |
| K28 | 00 51 42 | −71 59 52 | 2.10 ± 0.50 | −1.20 ± 0.20 | 9 |
| | | | 1.50 ± 0.60 | −1.00 ± 0.20 | 7 |
| K44 | 01 02 04 | −73 55 31 | 3.10 ± 0.80 | −1.10 ± 0.20 | 9 |
| HW 47 | 01 04 04 | −74 37 09 | 2.80 ± 0.90 | −1.00 ± 0.40 | 8 |
| HW 84 | 01 41 28 | −71 09 58 | 2.40 ± 0.20 | −1.20 ± 0.40 | 8 |
| HW 86 | 01 42 22 | −74 10 24 | 1.60 ± 0.20 | −0.75 ± 0.40 | 8 |
| BS 121 | 01 04 22 | −72 50 52 | 2.30 ± 0.20 | −1.20 ± 0.40 | 8 |
| BS 90 | 00 59 05 | −72 09 10 | 4.30 ± 0.10 | −0.84 | 10 |
| | | | $4.47^{+0.55}_{-0.49}$ | $-0.72^{+0.10}_{-0.13}$ | 11 |

Note.—Units of right ascension are hours, minutes, and seconds, and units of declination are degrees, arcminutes, and arcseconds.

References.—(1) Da Costa & Hatzidimitriou 1998; (2) Mighell et al. 1998; (3) de Freitas Pacheco et al. 1998; (4) Crowl et al. 2001; (5) Mackey & Gilmore 2003b; (6) Alves & Sarajedini 1999; (7) Piatti et al. 2005a; (8) Piatti et al. 2005b; (9) Piatti et al. 2001; (10) Sabbi et al. 2007; (11) this paper.

relaxation times, corresponding to the half-light and core radii, after we estimate the corresponding total and characteristic mass and the total number of stars within these radii. We find a half-mass relaxation time of $t_{\mathrm{rl},h} = 0.95 \pm 0.06$ Gyr and a core radius relaxation time of $t_{\mathrm{rl},c} = 0.33^{+0.06}_{-0.04}$ Gyr. From these timescales, which are much smaller than the evolutionary age of the cluster, we easily conclude that BS 90 is a dynamically relaxed spherical cluster, which thus exhibits the phenomenon of dynamical mass segregation.

## 7. CHEMICAL EVOLUTION HISTORY OF THE SMC

The chemical evolution history of a galaxy is understood in terms of the age-metallicity relation of both field and cluster stars. The chemical evolution histories in the Magellanic Clouds

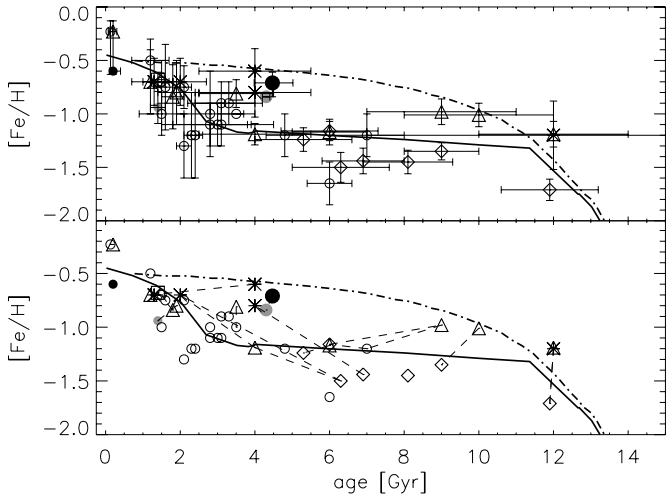


FIG. 10.—Age-metallicity relation of the cluster population in the SMC. The data are obtained from Crowl et al. (2001; *small gray dot*), Piatti et al. (2001, 2005a, 2005b; *small open circles*), Mighell et al. (1998; *diamonds*), Da Costa & Hatzidimitriou (1998; *triangles*), de Freitas Pacheco (1998; *asterisks*), Mackey & Gilmore (2003b; *small black dot*), Alves & Sarajedini (1999; *square*), and Sabbi et al. (2007; *large gray dot*). Our measurements for BS 90 are presented as the large black dot. In both panels the bursting (*solid curve*) and the smooth (*dot-dashed curve*) chemical evolution models by Pagel & Tautvaišienė (1998) are also shown. *Top*: The values for all studied SMC clusters (shown in Table 1) are plotted with their corresponding errors. *Bottom*: The same values from Table 1 are shown without their errors. The dashed lines connect the values from estimates derived from different studies for the same clusters, exhibiting, thus, the discrepancy in the results of different methods.

exhibit distinct features in comparison to that of the disk of the Milky Way (Westerlund 1997). Several models have been developed for their explanation, assuming bursts with IMFs steeper than Salpeter's IMF to produce subsolar metallicities (e.g., Russell & Dopita 1992; Tsujimoto et al. 1995) or postulating selective stellar outflows associated with star formation bursts (e.g., Pilyugin 1996). In contrast, the model of chemical evolution for the Magellanic Clouds developed by Pagel & Tautvaišienė (1998) assumes that the clouds have been built up by gradual infall of unprocessed material, linear laws of star formation, yields and time delays identical to those for the solar neighborhood, and a nonselective wind proportional to the star formation rate. These models represent chemical enrichment assuming a burstlike star formation ("bursting" model) and a continuous star formation rate over the entire lifetime of the SMC ("smooth" or simple "closed box" model).

In order to reproduce the age-metallicity relation for individual clusters in the SMC and add our results on BS 90, we collected a large set of data available on SMC clusters concerning their metallicities and ages. These data are given in Table 1. We plot the age-metallicity relation for the SMC clusters in Figure 10. The models published by Pagel & Tautvaišienė (1998) are also displayed with a solid (bursting model) and a dash-dotted line (smooth model). The top panel of Figure 10 shows ages and metallicities with the corresponding errors for all star clusters collected in Table 1. The bottom panel is displayed without the errors, but with a set of dashed lines, which show the connections of points derived from different studies for the same clusters. The latter shows that both the bursting and the smooth model can be supported by selecting certain clusters, and hence an unambiguous conclusion is not possible yet. Moreover, it should be noted that the data given in Table 1 consist of an inhomogeneous set of abundances, perhaps washing away any real effects. The transformation of all these results into a common spectroscopic scale would certainly provide a clearer picture. In any case, if we assume that the bursting model of Pagel & Tautvaišienė (1998) represents the chemical evolution history of the SMC, then our measurements reveal a relatively high metallicity for the epoch during which BS 90 was formed. These values seem to fit better the smooth model, which represents a continuous mode of chemical enrichment.

Indeed, our estimated age and metallicity for BS 90 places the cluster in Figure 10 closer to the smooth model (*large black dot*), in agreement with the estimations of Sabbi et al. (2007) (*large gray dot*). According to the bursting model an iron abundance of $[\mathrm{Fe/H}] \approx -1.2$ corresponds to a time around 4.5 Gyr ago. Our derived value for BS 90 is about 0.5 dex higher. On the other hand, the smooth model requires an iron content of $[\mathrm{Fe/H}] \approx -0.6$ at $\sim$4.5 Gyr, much closer to our derived value of $[\mathrm{Fe/H}] \approx -0.7$. A simple closed-box model is also supported by the results of Kayser et al. (2006) and consistent with the enrichment history of the outer SMC field, which has been derived by Dolphin et al. (2001). With its age and metallicity BS 90 adds an important point to the age-metallicity relation, which favors a continuous mode of chemical enhancement in the SMC, but the chemical evolution history of this galaxy still remains elusive and seems to be more complicated than reflected by the proposed models. Figure 10 also reveals an increasing number of clusters for the last $\sim$3 Gyr. This coincides with the increase of cluster formation in the LMC and is consistent with a close encounter between the Magellanic Clouds and Milky Way as proposed by Bekki et al. (2004). The strong tidal interactions could certainly trigger cluster formation.

## 8. SUMMARY

In this paper we have presented our detailed photometric analysis of the intermediate-age spherical star cluster BS 90 in the SMC.

We analyzed the stellar surface density profile of BS 90, following the models described by King (1962) and Elson et al. (1987). We derived almost the same value for the core radius of $r_c \simeq 5.5$ pc with both models. This value places BS 90 in the $r_c$-age relation among the SMC clusters that do not seem to evolve isolated. From the model of Elson et al. (1987), we found a stellar surface density that, at larger radii, decreases outward with a power-law slope of $\gamma \simeq 3.68$. The application of King's model delivered a tidal radius of $r_t \simeq 53.7$ pc and a concentration parameter $c \simeq 1.0$, which seems to be relatively low, compared to other SMC clusters (McLaughlin & van der Marel 2005).

We counted stars in different magnitude intervals in order to derive the LF of the cluster. The derived luminosity function of BS 90 reflects features of the cluster like the red clump as a higher stellar density around $V = 19$ mag and $I = 18.5$ mag and the turnoff at $V = 22$ mag and $I = 20.75$ mag. The PDMF is a linearly decreasing function up to the high-mass end of the cluster. We derived a slope of the PDMF of $a \simeq -0.95$ for a completeness in our photometry higher than 50% and of $a \simeq -1.30$ above the 70% completeness limit. Consequently, the PDMF of BS 90 has a slope between the one derived by Salpeter (1955) for the IMF in the solar neighborhood and a shallower slope, comparable to earlier derived slopes from studies on Magellanic Cloud clusters (e.g., Kerber & Santiago 2006; Gouliermis et al. 2004). The difference from the Salpeter slope can also be explained by the fact that unresolved binaries flatten the PDMF (Kerber & Santiago 2006) or that stars escaped from the cluster (Meylan & Heggie 1997).

We investigated the radial dependence of the MF slope to check whether BS 90 is mass segregated or not. We found that indeed the MF becomes steeper at larger distances from the center of the

cluster. The radial dependence of the slope indicates a central concentration of the massive stars and hence mass segregation. We also confirm previous claims that the PDMF around the half-mass radius is comparable to the overall PDMF since it is the region that is least affected by mass segregation (Kroupa 2002; Vesperini & Heggie 1997). Within the half-light radius of $\simeq$9.4 pc, we obtained a half-mass relaxation time of about 0.95 Gyr and therefore we conclude that the mass segregation is due to the dynamical evolution of BS 90, since the age of the cluster is older than the derived half-mass relaxation time. Mass segregation provides another possible reason for a flattening of the MF that may occur during the evolution of the cluster.

Isochrone models fitted to the constructed CMD (Fig. 6) of BS 90 revealed an age of about 4.5 Gyr, which characterizes this cluster as one of the very rare star clusters formed in a possible quiescent period of cluster formation in the SMC (Rafelski & Zaritsky 2005). There are only a few clusters in the range between 4 and 10 Gyr. The applied isochrone yields a metallicity of $[\mathrm{Fe/H}] \simeq -0.72$. The total visual extinction has been found to be $A_V \sim 0.04$ mag. The low value of the total visual extinction combined with the large amount of gas in the general region and the absence of indications of differential reddening in the CMD of BS 90 suggests that the cluster is probably located in front of the association NGC 346. The distance of BS 90 has been estimated to $\simeq$58.9 kpc.

The location of BS 90 in the age-metallicity plot shows that this cluster fits better a simple "smooth" model that represent a continuous chemical enhancement for the SMC, rather than a "bursting" model of the chemical evolution history of the galaxy, in agreement with recent results on other SMC clusters (Kayser et al. 2006). However, inconsistent metallicity estimation methods for different SMC clusters provide an inhomogeneous set of results that should be transferred onto a common abundance scale, so that an unambiguous picture of the chemical evolution history of SMC can be derived. Furthermore, given that the SMC is part of an interacting system between the Magellanic Clouds and the Milky Way, the chemical evolution history of this galaxy is probably far more complicated than what is suggested by a simple "closed box" model.

Dimitrios A. Gouliermis acknowledges the support of the German Research Foundation (Deutsche Forschungsgemeinschaft) through the individual grant 1659/1-1. Boyke Rochau would like to thank Sascha P. Quanz and Alessandro Berton for their helpful suggestions. This paper is based on observations made with the NASA/ESA *Hubble Space Telescope*, obtained from the data archive at the Space Telescope Science Institute. STScI is operated by the Association of Universities for Research in Astronomy, Inc., under NASA contract NAS5-26555.

## REFERENCES

Alves, D. R., & Sarajedini, A. 1999, ApJ, 511, 225
Baumgardt, H., & Makino, J. 2003, MNRAS, 340, 227
Bekki, K., Couch, W. J., Beasley, M. A., Forbes, D. A., Chiba, M., & Da Costa, G. S. 2004, ApJ, 610, L93
Bertelli, G., Bressan, A., Chiosi, C., Fagotto, F., & Nasi, E. 1994, A&AS, 106, 275
Bica, E. L. D., & Schmitt, H. R. 1995, ApJS, 101, 41
Binney, J., & Merrifield, M. 1998, Galactic Astronomy (Princeton: Princeton Univ. Press)
Binney, J., & Tremaine, S. 1987, Galactic Dynamics (Princeton: Princeton Univ. Press)
Crowl, H. H., Sarajedini, A., Piatti, A. E., Geisler, D., Bica, E., Clariá, J. J., & Santos, J. F. C., Jr. 2001, AJ, 122, 220
Da Costa, G. S. 1991, in IAU Symp. 148, The Magellanic Clouds, ed. R. Haynes & D. Milne (Dordrecht: Kluwer), 183
Da Costa, G. S., & Hatzidimitriou, D. 1998, AJ, 115, 1934
de Freitas Pacheco, J. A., Barbuy, B., & Idiart, T. 1998, A&A, 332, 19
de Grijs, R., Gilmore, G. F., Johnson, R. A., & Mackey, A. D. 2002, MNRAS, 331, 245
Dolphin, A. E. 2000, PASP, 112, 1383
Dolphin, A. E., Walker, A. R., Hodge, P. W., Mateo, M., Olszewski, E. W., Schommer, R. A., & Suntzeff, N. B. 2001, ApJ, 562, 303
Elson, R. A. W., Fall, S. M., & Freeman, K. C. 1987, ApJ, 323, 54 (EFF)
Girardi, L., et al. 2002, A&A, 391, 195
Gouliermis, D., Keller, S. C., Kontizas, M., Kontizas, E., & Bellas-Velidis, I. 2004, A&A, 416, 137
Gouliermis, D. A., Dolphin, A. E., Brandner, W., & Henning, T. 2006, ApJS, 166, 549 (Paper I)
Henize, K. G. 1956, ApJS, 2, 315
Kayser, A., Grebel, E. K., Harbeck, D. R., Cole, A. A., Koch, A., Gallagher, J. S., & Da Costa, G. S. 2006, preprint (astro-ph/0607047)
Kerber, L. O., & Santiago, B. X. 2006, A&A, 452, 155
King, I. 1962, AJ, 67, 471
Kroupa, P. 2002, Science, 295, 82
Lightman, A. P., & Shapiro, S. L. 1978, Rev. Mod. Phys., 50, 437
Mackey, A. D., & Gilmore, G. F. 2003a, MNRAS, 338, 85
———. 2003b, MNRAS, 338, 120
Mackey, A. D., & Gilmore, G. F. 2003c, MNRAS, 340, 175
Mackey, A. D., Payne, M. J., & Gilmore, G. F. 2006, MNRAS, 369, 921
McLaughlin, D. E., & van der Marel, R. P. 2005, ApJS, 161, 304
Meylan, G., & Heggie, D. C. 1997, A&A Rev., 8, 1
Mighell, K. J., Sarajedini, A., & French, R. S. 1998, AJ, 116, 2395
Nazé, Y., Hartwell, J. M., Stevens, I. R., Manfroid, J., Marchenko, S., Corcoran, M. F., Moffat, A. F. J., & Skalkowski, G. 2003, ApJ, 586, 983
Nazé, Y., Manfroid, J., Stevens, I. R., Corcoran, M. F., & Flores, A. 2004, ApJ, 608, 208
Pagel, B. E. J., & Tautvaišiené, G. 1998, MNRAS, 299, 535
Peimbert, M., Peimbert, A., & Ruiz, M. T. 2000, ApJ, 541, 688
Piatti, A. E., Santos, J. F. C., Clariá, J. J., Bica, E., Ahumada, A. V., & Parisi, M. C. 2005a, A&A, 440, 111
Piatti, A. E., Santos, J. F. C., Clariá, J. J., Bica, E., Sarajedini, A., & Geisler, D. 2001, MNRAS, 325, 792
Piatti, A. E., Sarajedini, A., Geisler, D., Seguel, J., & Clark, D. 2005b, MNRAS, 358, 1215
Pilyugin, L. S. 1996, A&A, 310, 751
Rafelski, M., & Zaritsky, D. 2005, AJ, 129, 2701
Rich, R. M., Shara, M., Fall, S. M., & Zurek, D. 2000, AJ, 119, 197
Rubio, M., Contursi, A., Lequeux, J., Probst, R., Barbá, R., Boulanger, F., Cesarsky, D., & Maoli, R. 2000, A&A, 359, 1139
Russell, S. C., & Dopita, M. A. 1992, ApJ, 384, 508
Sabbi, E., et al. 2007, AJ, 133, 44
Salpeter, E. E. 1955, ApJ, 121, 161
Scalo, J. M. 1986, Fundam. Cosmic Phys., 11, 1
Spitzer, L. 1975, in IAU Symp. 69, Dynamics of Steller Systems, ed. A. Hayli (Dordrecht: Reidel), 3
———. 1987, Dynamical Evolution of Globular Clusters (Princeton: Princeton Univ. Press)
Tsujimoto, T., Nomoto, K., Yoshii, Y., Hashimoto, M., Yanagida, S., & Thielemann, F.-K. 1995, MNRAS, 277, 945
van den Bergh, S. 1991, ApJ, 369, 1
Vesperini, E., & Heggie, D. C. 1997, MNRAS, 289, 898
Westerlund, B. E. 1997, The Magellanic Clouds (Cambridge: Cambridge Univ. Press)